Brittle to Quasi-Brittle Transition and Crack Initiation Precursors in Crystals with Structural Inhomogeneities

S. Papanikolaou^{a*}, P. Shanthraj^c, J. Thibault^a, C. Woodward^b, F. Roters^c

AUSI

Article Info Keywords: Microstructural Disorder Crack Nucleation Surface Fractal Topography Crack Initiation DAMASK Avalanches

Abstract

Crack initiation emerges due to a combination of elasticity, plasticity, and disorder, and it displays strong dependence on the material's microstructural details. The characterization of the structural uncertainty in the original microstructure is typically empirical and systematic characterization protocols are lacking. In this paper, we propose an investigational tool in the form of the curvature an ellipsoidal notch: As the radius of curvature at the notch increases, there is a dynamic phase transition from notch-induced crack initiation to bulk-disorder crack nucleation. The notch length scale associated with this transition may provide an additional characteristic of the original material microstructure. We investigate brittle but elastoplastic metals with coarse-grained, microstructural disorder that could originate in a material's manufacturing process, such as alloying. We perform extensive and realistic simulations using a phase-field approach coupled to crystal plasticity. The microstructural disorder and notch width are systematically varied. We identify this transition for various disorder strengths in terms of the damage evolution. We identify detectable precursors to crack initiation that we quantify in terms of the expected stress drops during mode I fracture loading. Finally, we discuss ways to observe and analyze this brittle to quasi-brittle transition in experiments.

1 Introduction

Fracture mechanics of intermetallic materials and other alloys and superalloys remains a critical topic of discussion in the research of mechanical fatigue failure and fracture. The necessity of intermetallics and superalloys originated in their use for high-temperature applications and components such as gas turbine blades and automobiles (Clemens and Mayer 2013, Stoloff et al. 2000, Kim 1994, and Kim and Dimiduk 1991). Since then, potential applications have spanned from the aerospace industry to electronic devices. While the alloying process may cause excellent mechanical properties like increased oxidation resistance and resistance to creep, it, also, naturally introduces uncertainty in the form of quenched disorder in the material microstructure. For example, ranging over several orders of magnitude, intermetallics display several characteristic length scales which govern material strength properties (see Appendix A) (Campbell et al. 1999, Dimiduk 1999, Kim 1994, and Kim and Dimiduk 1991). For example, in Titanium Aluminide (TiAl) based alloys, grain sizes can be as small as 2 microns (for fine-grained Ti-rich Ti-Al alloy compacts) due to powder metallurgical processes (Vajpai and Ameyama 2013 and Lapin 2009) and as large as 800 microns due to conventional casting methods and additional alloy compounds like TiB₂ (see Appendix A) (Han et al. 2015 and Hu 2001). Similar to TiAl, Nickel Aluminide (NiAl)-based alloys and Inconel express similar microstructural lengthscale characteristics on the same orders of magnitude (see Appendix A) (Zhu et al. 2018 and Herbold et al. 2011). Due to the very presence of this structural disorder, such alloys display stochastic fracture characteristics, especially when cracks are short enough. It is characteristic that the range of fatigue crack growth rates for short cracks can extend well beyond 4 orders of magnitude (approximately 10⁻¹¹ to 10⁻⁶ m/cycle) (see Appendix B) (Ritchie and Peters 2001). It is natural to interpret these wide-ranging short crack-growth rates as being an outcome of the alloying disorder and thus, may be associated to avalanche precursors of cracking in fatigue, analogous to other avalanche precursors in various complex systems (Papanikolaou et al. 2018). In parallel to identifying fracture-

-

^aBenjamin M. Statler College of Engineering, West Virginia University, Morgantown, WV 26505, USA

b Materials and Manufacturing Directorate, Air Force Research Laboratory, Wright Patterson Air Force Base, Dayton, OH 45433-7817, USA

^cMax-Planck-Institut für Eisenforschung, Max-Planck-Straße 1, 40237 Düsseldorf, Germany

^{*} Corresponding Author e-mail: stefanos.papanikolaou@mail.wvu.edu

predicting precursors, the quenched disorder characteristics are expected to evolve with fatigue loading in a way that has not yet been studied in detail. In this paper, we discuss in detail how such stochastic fracture, and its avalanche precursors, can emerge in a model material with relatively realistic parameters and we explore the possibility of characterizing and quantifying the structural disorder in a statistical manner by locating a naturally-occuring brittle to quasibrittle dynamical phase transition.

Microstructural heterogeneity is an unavoidable effect that originates in the multiple processes used to combine materials towards manufacturing an alloy. In analogy to other disordered many-body systems, it is natural to envision that this material heterogeneity gives rise to abrupt crack growth events, especially at short length scales compared to the microstructural heterogeneity. Given the limited statistical sampling of short crack growth in mechanical components, it is imperative to clarify ways and protocols that can capture, controllably and systematically, this precursor behavior to fracture. We envision an experimental protocol for identifying and controlling the onset of such precursor events. In order to pursue such a protocol, we utilize a model material which could be considered a simplification of an intermetallic alloy. It is well recognized that alloys such as NiAl may contain multiphase variability at a length scale of a few microns as a result of alloying processes (Wang et al. 2016, Herbold et al. 2011, and Lay and Yavari 1996). We model this structural disorder in terms of the local propensity for damage and we use a continuous approach, by taking into account that macroscale fracture of such alloys is typically brittle at room temperature, while in the micron and submicron scale one can identify primarily plastically deforming materials. Therefore, it is natural to first pursue the understanding of crack growth in brittle fracture as it competes with crystal plasticity at the microscale; this is precisely the character of the model we consider in this work.

The statistical effects of material heterogeneity in short-crack growth for alloys and superalloys have remained elusive: While it is well known how alloying processes produce several precipitates such as γ' and γ'' phases which may directly affect local material strength properties (Tian et al. 2014), it is unknown how they influence the probability of large or small crack growth "bursts" as a fatigue cycle proceeds. Motivated by basic elastic fracture mechanisms (Zehnder 2012), it is natural to refer to the so-called "quasi-brittle" fracture, which is motivated by large-scale fracture of disordered specimens, such as concrete. Early experiments of fracture on concrete did not obey the criteria that characterize Linear Elastic Fracture Mechanics (LEFM) (Walsh 1972). Through many experiments (Grote et al. 2001, Schlangen 1993, Schlangen and Van Mier 1992, and Bazant and Pfeiffer 1985), it was concluded that a nonlinear approach for predicting fracture in these materials with a heterogeneous mesostructure is essential to understanding and characterizing this deviant fracture behavior. Many numerical methods were developed to characterize the experimental data and predict with accuracy these fracture characteristics (Schlangen and Garboczi 1997, Bazant et al. 1990, and Bazant and Oh 1983). While material heterogeneity of rock, concrete, wood and ice are considered at large length scales on the order of a few millimeters (Skarynski and Tejchman 2010), analogous results can be considered mutatis mutandis for smaller scale disorder in alloys and superalloys.

Quasibrittle materials contain inhomogeneities that cannot be considered negligible when compared to the structure size (Bazant et al. 2009). As a result, the fracture strength of a structure can depend greatly on its size. This phenomenon, typically referred to as size effect, has been observed in many materials from bone (Evans 1973) to concrete (Bazant 1984). However, alloys and superalloys display similar fracture characteristics at much smaller scales, such as a few microns. If both concrete and alloys share similar fracture characteristics, then it is natural to investigate whether scaling relations for quasibrittle materials may be applied to alloy-relevant smaller length scales. For example, in Refs. [(Bazant and Planas 1998, Bazant 1996, and Bazant and Li 1996)], it was suggested that quasibrittle materials can be characterized using a scaling relation for which fracture strength could be predicted with statistical accuracy.

$$\sigma_F = B f_t' \left(1 + \frac{d}{d_0} \right)^{-1/2} \tag{1}$$

This scaling relation can be derived by asymptotic matching of the fracture stress as a function of size, represented in Equation (1) where σ_F is the fracture strength, B is a dimensionless constant, f'_t is the tensile strength, d_0 is a constant referred to as the transitional size, and d is the characteristic size of the structure (Bazant 1985 and Bazant 1984). Is such a scaling relation valid for superalloys and intermetallics? We wish to apply such a methodology to characterize disorder in our model material and also identify additional statistical representations. It is a purpose of this manuscript to contribute to the analysis and characterization of quasibrittle material at small length scales.

Our methodology is also based on the possible and viable ways to classify this short crack growth regime by developing an experimental protocol that produces a transition in fracture behavior. Due to advances in microfabrication techniques, namely focused ion beam (FIB), it is now possible to machine precise-dimensioned notches at the micron and submicron scale to a sub-10nm resolution (Ochiai et al. 2010 and Tseng 2004). If we consider integrating this technique into an experimental protocol, it is realistic to envision high-throughput experiments where one machines and tests various notch curvatures in order to observe the variety of patterns in fracture behavior. We pursue the direction of modifying the curvature of a fixed-depth notch where it is naturally expected that the notch will influence fracture only after it becomes sharp enough, defining a quasibrittle to brittle transition as a function of notch curvature. At which lengthscale does the material disorder cause a transition from brittle to quasibrittle fracture behavior? Is it possible to characterize this transition as a function of the notch curvature? These are question that we address in this paper.

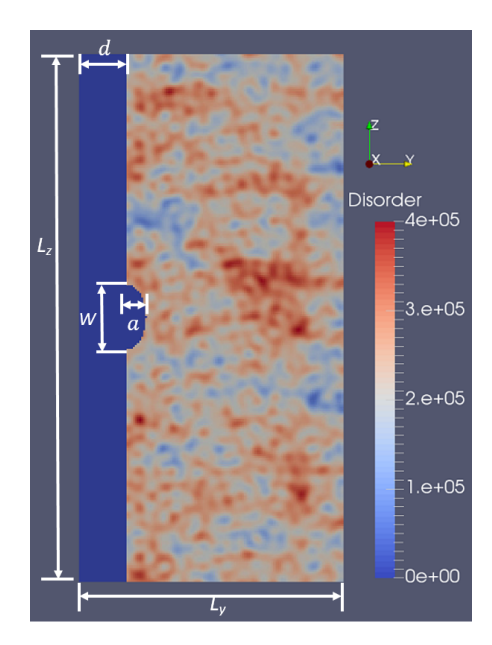


Figure 1: Model Geometry & Disorder: A disorder strength of R_G =0.2 was chosen where the thickness of the sample, L_x is 8 μ m, the width of the sample, L_z , is 1.0 mm, the length of the sample, L_y , is 0.5 mm, W is the initial crack width is 128 μ m, d is 96 μ m, and d is the constant major axis of 64 μ m.

Crack initiation from a notch is commonly believed to be controlled by pure elasticity. However, heterogeneous materials contain inhomogeneities that can contribute as much to fracture as a notch. Therefore, if the curvature of the notch softens, the stresses at the notch root will decrease and, as a result, redistribute within the bulk of the material. This will allow for a natural competition of fracture between the notch and the microstructural heterogeneity. While research of notched, brittle materials has been studied for decades, the effects of a notched geometry in heterogeneous materials has

been of more recent focus. Given their increased use in industrial applications, it is important to understand how fracture behaves for these types of materials. To this end, we model a disordered specimen with variance in its fracture strength properties, yielding fracture characteristics that follow the quasibrittle regime. It is believed that predicting fracture characteristics requires developing scaling relationships that bridge the LEFM regime to the plastic regime through asymptotic matching (Bazant and Yu 2004). It is this kind of scaling relationships that we wish to pursue for microstructurally small cracks in alloys and superalloys, in order to identify the main structural inhomogeneity length scales.

In this paper, we simulate a transition from notch-driven crack initiation, characteristic of LEFM, to bulk crack nucleation, characteristic of quasibrittle fracture, using a model material that resembles a brittle material that may plastically deform at the microscale. We use an integrated spectral phase field approach coupled constitutively to elastoplasticity through the Düsseldorf Advanced MAterial Simulation Kit, DAMASK, software (Roters et al. 2019). Elasticity and crystal plasticity are modeled through typical constitutive laws that take into account grain orientation, crystalline structure, and possible slip systems (Asaro 1983). Through the application of this multiscale, micromechanical analysis, the microstructure can be linked to the macroscopic response. In this paper, we perform extensive simulations of a notched specimen with dimensions: $L_x \times L_y \times L_z$. The test samples have an assumed length scale of 1 mm per 256 units (essentially, each unit corresponds to $\sim 4 \mu m$). L_x and L_z are held constant at 8 μm and 1.0 mm, respectively. L_y is varied from 0.25 mm to 1.0 mm. The ellipsoidal notch is placed along the y-axis at the edge of the specimen where the major axis, $a=L_v/8$, is held constant. However, in order to observe the transition from notch-driven crack initiation to bulk-induced crack nucleation, the notch width, W, is varied at values from 16 μm to 0.5 mm, increasing the radius of curvature. In order to modify in a generic fashion the microstructural propensity to fracture and introduce a particular disorder lengthscale, we consider quenched stochastic contribution in the *local* critical strain energy release rate that controls the rate of local damage accumulation. Defining the ratio of the variance ratio of this disorder parameter as R_G, we consider a large but relevant parameter range. For the generation of spatially stochastic but continuous variables, a Weierstrass-Mandelbrot function (Shanthraj et al. 2011) in which the fractal dimension, D, is either 2.85 or 2.995. As shown in Figure 1, the sample has an induced disorder distribution in a phase feature, that varies a parameter which we only consider in the phase-field damage evolution, according to the parameters and dimensions aforementioned. For every R_G , high-throughput simulations (>20 realizations per case) are performed in order to take into account stochastic microstructure fluctuations.

In section 2, we explain how the disorder distribution is generated and the algorithmic structure of DAMASK. Also, we discuss the phase field approach solves for damage evolution. In section 3, we discuss the simulation results and how: a) D influences the fracture behavior, b) induced-disorder affects the location of crack nucleation, and c) the introduction of a notch affects crack initiation. Furthermore, we discuss how the transition from notch-driven crack initiation to bulk-disorder crack nucleation indicates a transition from brittle to quasi-brittle fracture regimes. Finally, in section 4, we present our conclusions about the importance of this work and possible future directions.

2 The Model: Material disorder, phase-field damage and crystal plasticity

DAMASK utilizes a phase field model in the continuum to develop constitutive laws towards solving for material deformation due to the damage evolution within the sample. It uses a spectral method to solve for the elastic and plastic deformation with Fast Fourier transforms (FFT). Fourier methods require a rectangular-gridded mesh and periodic boundary conditions. Therefore, we apply a layer of air in contact with the notched surface, in order to satisfy the periodic boundary conditions. In this section, we discuss: the phase field approach, the structure of the material point model, and how the disorder of the material is generated.

2.1 Phase Field Approach

For the investigation of cracks, DAMASK utilizes a phase field approach (Aranson et al. 2000) where cracks are modeled by a phase with order parameter $\phi = 0$, while the material has $\phi = 1$. ϕ couples proportionally to the elastic coefficients of the material, softening it as it is damaged. DAMASK utilizes a spectral method to resolve the elastic, plastic and damage equations during crack growth. The material point model rationalizes the elastic and plastic effects in order to observe how damage evolves (see Appendix D). The method for modelling damage in the phase field uses free energy equations to determine if certain criterion is met. The thermodynamically consistent free energy form is used.

$$\psi = \psi_E + \psi_D + \psi_P \tag{2}$$

Where ψ_E , ψ_D , and ψ_P are the elastic, damage, and plastic free energy contributions, respectively.

Elastic free energy is quite prevalent within the sample as it is loaded. The elastic energy is decomposed in a direct multiplicative manner to the simplest damage contribution (ϕ^2) and a pure distortion-dependent contribution:

$$\psi_E = \phi^2 \widetilde{\psi_E} (\nabla X, F_p) \tag{3}$$

At the undamaged state where damage hasn't occurred, the sole energy contribution to the sample is elastic free energy. In equation 4, it is a function of the stored elastic energy density, $\widetilde{\psi}_E$, and the phase field. The stored elastic energy density is dependent on the product of the dissipation potential, X, and plastic deformation. As the loading progresses, the strain energy release rate, G, reaches a critical point where the elastic free energy in the disordered distribution, locally, is converted to plastic free energy. The critical strain energy release rate, G_c , is how the model determines if permanent deformation has occurred. Locally, these areas will only exhibit damage and plastic free energy (Shanthraj et al. 2016).

The damage accumulation is determined by the Fourier grid variables as the critical strain energy release rate values are assigned. As the strain is increased, the mesh is used to track all respective energy contributions at each incrementally-increasing strain-steps. With this progression, there is deformation in the sample that can be quantified. Damage is modelled using an isotropic brittle model based on rupture criterion where elastic strain energy, G, is the driving parameter for determining damage, ϕ : $\phi_l = G_c/G$. ϕ_l is local damage. The damage free energy is nonzero only after the crack initiation event,

$$\psi_D = \frac{1}{2} G_c l |\nabla \phi|^2 + \frac{G_c}{l} (1 - \phi)^m + I_{[0,1]}(\phi)$$
(4)

Where G_c and l are material constants and m is the order of the phase field potential. Equation 5 represents how the damage free energy is determined. G_c is the critical strain energy release rate, analogous to the work of fracture. In our field model, this amounts to the free energy contribution necessary for crack nucleation to occur, and l is the resolution length scale which should correspond to a representative volume element (RVE) of the material (Shanthraj et al. 2016). In our simulations, we consider a fixed resolution length equal to 4 mesh units, which corresponds to $\sim 16 \mu m$, given our considered sample dimensions. As damage evolves, there is a permanent deformation that, also, contributes to plastic free energy.

As analysis of the plastic free energy is quite nontrivial. Physically, it only occurs at the crack initiation and propagation areas. Furthermore, these are places at which permanent deformation occurs. Quantifying the plastic free energy involved requires an indirect approach. We must first solve for the total free energy.

$$\partial \mathbf{F}_n \psi = -\phi^2 \mathbf{S} \mathbf{F}^{-T} \tag{5}$$

However, we must reduce and simplify this equation into the familiar slip system based conjugate pair.

$$-\partial \mathbf{F}_{n}\psi \cdot \dot{\mathbf{F}}_{n} = \sum_{\alpha} \partial \gamma^{\alpha} \psi \dot{\gamma}^{\alpha}, \tag{6}$$

where

$$\partial \gamma^{\alpha} \psi = -\phi^{2} \mathbf{S} \cdot (\mathbf{S}^{\alpha} \otimes \mathbf{n}^{\alpha}) = \tau^{\alpha} \tag{7}$$

As it can be seen, the plastic free energy is a function of several important parameter. It is necessary to consider the constitutive plasticity equation in order to solve for these parameters. The constitutive law of plasticity for the plastic velocity gradient use the second Piola-Kirchhoff stress. The slip rate, $\dot{\gamma}^{\alpha}$, is a function of S, and L_p is a function of this slip rate.

$$L_{p} = \sum_{\alpha} \dot{\gamma}^{\alpha} \mathbf{s}^{\alpha} \otimes \mathbf{n}^{\alpha} \tag{8}$$

Where s and n being the unit vectors along the slip direction and slip plane normal, respectively, and α is the index of a slip system. We consider all 12 FCC slip systems which may become active in our single crystal with fixed crystalline orientation. However, the slip rate is guided by the basic phenomenological crystal plasticity constitutive equation.

$$\dot{\gamma}^{\alpha} = \dot{\gamma}_{o} \left| \frac{\tau^{\alpha}}{g^{\alpha}} \right|^{n} sgn(\tau^{\alpha}) \tag{9}$$

Where $\dot{\gamma}_o$ is the reference shear rate, $\tau^\alpha = \mathbf{S} \cdot (\mathbf{s}^\alpha \otimes \mathbf{n}^\alpha)$, n is the stress exponent and g^α is the slip resistance stress for a slip system α . The hardening law is:

$$\dot{g}^{\dot{a}} = \sum_{\beta=1}^{12} \dot{\gamma^{\dot{\beta}}} h_0 \left| 1 - \frac{g^{\beta}}{g_{\infty}^{\alpha}} \right|^{w} sgn \left(1 - \frac{g^{\beta}}{g_{\infty}^{\alpha}} \right) h_{\alpha\beta}$$
 (10)

Where w and h_0 are hardening parameters, g_{∞}^{α} is the saturation stress, and $h_{\alpha\beta}$ is the hardening matrix which captures the interactions between different slip systems (Shanthraj et al. 2016). Once these parameters and equations are resolved and the plastic velocity gradient can be used to solve for the plastic deformation gradient: $\dot{F}_p = L_p F_p$. Once the total free energy is solved for, we can rearrange Equation 3 to find the plastic free energy of the sample. While it is useful to consider all contributions of free energy to the phase field, this model mainly focuses whether criterion is sufficiently satisfied to assign damage to units on the Fourier grid.

2.2 Heterogeneous Microstructure Generation

In this work, we identify disorder in terms of the variability for the critical strain energy release rate G_c . We assume throughout that G_c displays local, quenched and continuous fluctuations, as it would naturally happen in a multi-phased disordered metal alloy or a fatigued specimen. Namely, we assume that $\delta G_c \to \langle G_c \rangle + \Delta G_c(y,z)$ and the local fluctuations $\Delta G_c(y,z)$ are given in space through the aforementioned W-M function with an autocorrelation lengthscale of 160 microns at a given fractal dimension D. The critical experimentally relevant parameter in these simulations is the degree of relative disorder fluctuations, or in other words the width of the distribution of G_c with respect to the average critical strain energy release rate. If we define the standard deviation of the distribution as δG_c , then the important quantity to investigate would be $R_G = \delta G_c/\langle G_c \rangle$. In the next section, we discuss how this phase field model in a realistic elastoplastic environment can cause crack initiation and fracture at various notch widths and disorder strengths, keeping $\langle G_c \rangle$ fixed but changing the disorder ratio R_G .

The heterogeneity of the sample is considered as the induced disorder of material bulk. The Weierstrass-Mandelbrot (W-M) function allows for modeling of such macrostructural disorder using microscopic roughness in the energy required for local damage to statistically quantify microstructural imperfections. More specifically, it creates a Gaussian distribution of this fluctuating energy (Weierstrass 1895 and Mandelbrot 1979).

$$\Delta G_c(y,z) = L \left(\frac{G}{L}\right)^{D-2} \left(\frac{\ln \gamma}{M}\right)^{1/2} \sum_{m=1}^{M} \sum_{n=0}^{n_{max}} \gamma^{(D-3)n} \times \left\{ \cos(\phi_{m,n}) - \cos\left[\frac{2\pi \gamma^n (y^2 + z^2)^{1/2}}{L} \times \cos\left(\right. \right. \right. \right. \\ \left. + \cos\left(\frac{z}{y}\right) - \frac{\pi m}{M}\right) + \phi_{m,n} \right] \right\} (11)$$

Within the W-M function (Eqn. 2), the parameter, G, is defined as the variance of the spatial fluctuations, and the fractal dimension, D, exhibits a strong influence over the spatial fluctuations in the energy and stochastic characteristics. Therefore,

the critical parameters that cause the most stochastic changes and effects the crack growth and damage evolution are G and D (Mandelbrot et al. 1984, Shanthraj et al. 2011, and Carney and Mecholsky 2013). However, there are other parameters that help manipulate the fracture behavior: L is the sample length, γ is a scaling parameter, M is the superposed ridges used to construct the surface for its roughness, $\varphi_{m,n}$ is a random phase with m and n defining the ridge and frequency index, n is a frequency index that must control the max index considered, $\Delta G_c(y,z)$ is the fluctuational critical strain energy release rate, and y [m] and z [m] correspond to locations in the Fourier grid. The W-M function is used to manipulate the critical strain energy release rate, G_c , distribution of the sample and provides a statistical disorder distribution in order to simulate fracture behavior.

3 Simulation Results

The objective of the simulations is to identify the characteristic effect of the stochastic local damage distributions and how they contribute to the fracture mechanics of the specimen. When crack initiation occurs, the natural outcome is to occur at the notch for brittle materials, given that the stress profile is far higher at the notch tip than any place in the bulk, allowing failure to occur at this point. However, the induced disorder distribution in the specimen could allow for crack nucleation away from the tip of the notch. The material parameters (Table 1) of the model will drive such stochastic behavior.

| Property | Value (Model Material) | Units |
|------------------|------------------------|-----------------|
| C ₁₁ | 106.75 | GPa |
| C_{12} | 60.41 | GPa |
| C ₄₄ | 28.34 | GPa |
| $\dot{\gamma}_0$ | 1.0×10^{-3} | s ⁻¹ |
| n | 20 | |
| ${g}_0$ | 31 | MPa |
| g_{∞} | 63 | MPa |
| a | 2.25 | |
| h_0 | 75 | MPa |
| 1. | 0 | |

 $h_{\alpha\beta}$ 0 Table 1: Phase parameters used in the simulations for the model material (Tikhovskiy et al. 2007).

Where C_{11} , C_{22} , and C_{44} are elastic constants. These parameters are used in the constitutive elastic and plastic equations in order to determine the deformation on the sample.

The fractal dimension D is a free parameter of our simulations that plays an important role in the disordered fracture energy profile and is used in the W-M function. D is adjusted in order to increase the fluctuation in the local critical strain energy release rate, δG_c , but also make sure that he discretization unit of the simulation is smaller than either the disorder lenghscale or the lengthscale associated with the notch curvature (see Appendix C). With the increase in fractal dimension, the crack nucleates away from the notch at lower disorder strengths because the critical strain energy release rate varies at a higher degree for lower disorder strengths compared to the lower fractal dimension. Simulations (not shown) were conducted at several fractal dimension values to determine a particularly chosen value for D(=2.85) so that the fluctuations in the critical strain energy release rate would affect the crack nucleation and propagation behavior.

The competition between the length scale of damage spatial fluctuations (due to spatially varying δG_C) with the length scale associated with the notch, becomes evident in the increase of the notch curvature. Figure 2 shows the damage (where 1 is undamaged and 0 is fully damaged) and stress (Pa) distributions for initial crack widths of 16 μ m, 128 μ m, and 0.5 mm.

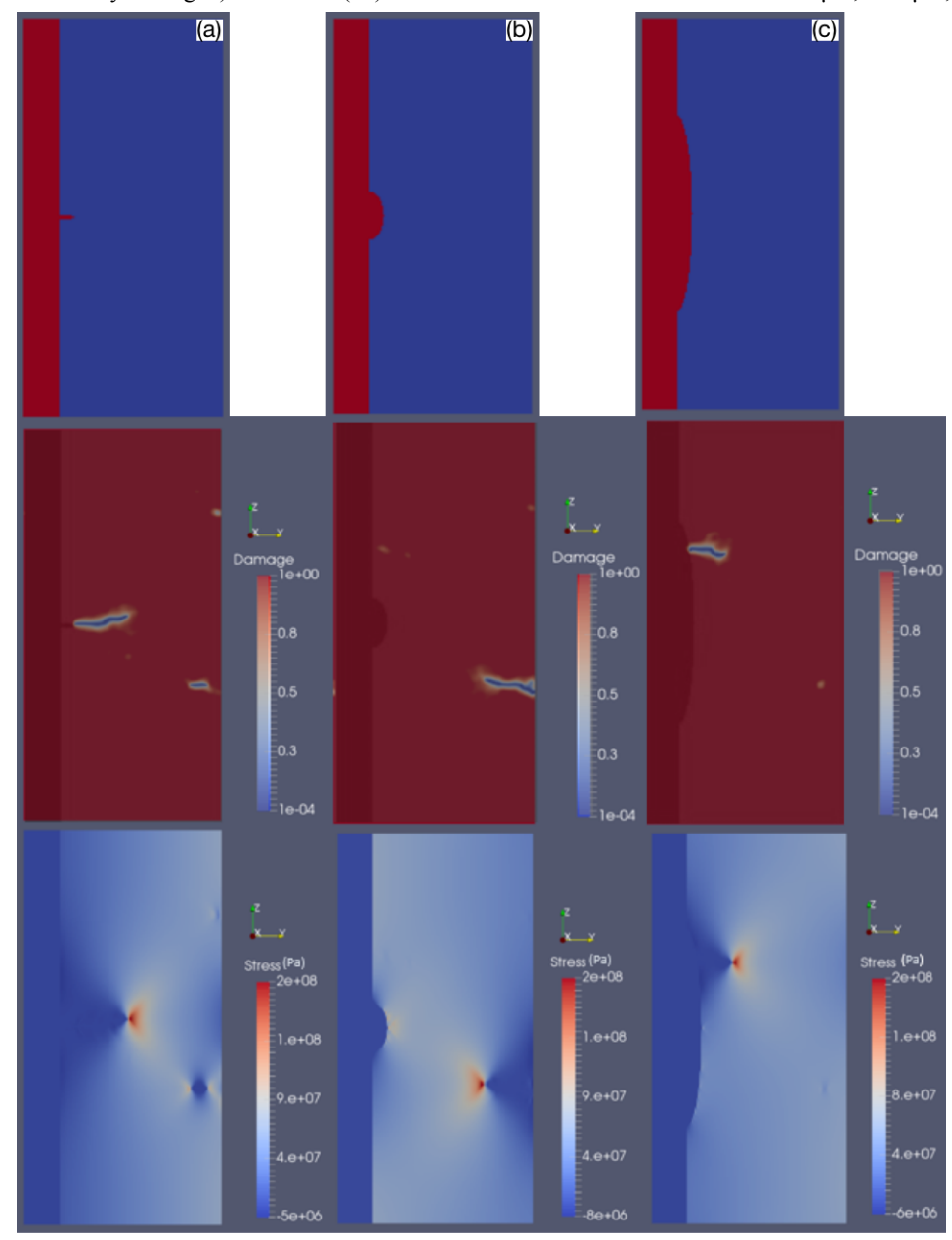


Figure 2: Effect of increasing notch width on crack nucleation for fractal dimension D=2.85: Simulations of system size of L_x =8 μ m, L_y = 0.5 mm, and L_z =1.0 mm where D=2.85, R_G = 0.8, and (a) has a W of 16 μ m (b) has a W of 128 μ m (c) has a W of 0.5 mm where the texture, damage and stress (along the loading direction σ_{zz}) distributions are displayed,

Though there is a transition from notch-located crack initiation to bulk material crack nucleation, this behavior occurred at

a disorder ratio R_G of 0.8 where the material fluctuations are the largest on the tested interval. When the fractal surface roughness is increased, this fracture behavior occurs at disorder ratios of approximately \sim 0.2, much lower in the tested interval. At a disorder of 0.8 for the higher fractal dimension, the specimens produce multiple nucleation points with larger values of damage. Nevertheless, at lower fractal dimension D = 2.85, the crack propagation is quite brittle with almost no branches of secondary cracks form.

In general, it is natural to expect that the simulation results are overall independent of the damage distribution's fractal dimension, and for this reason we will be only studying two cases throughout this work (D=2.85 and 2.995). However, the fractal dimension is also crucial in bypassing the mesh discretization resolution, which naturally leads to artificial stress concentrations near the engineered ellipsoidal notch.

3.1 Crack initiation for fixed notch width as function of increasing *local* critical strain energy release rate's variance

Analogously to other works (Bazant et al. 1998) and (Alava et al. 2008), the increase of disorder leads to the onset of quasi-brittle behavior, namely crack nucleation initiates at bulk locations, where the weakest sites exist. Here, we investigate this phenomenon in the presence of a notch, and in the context of our simulation software DAMASK and through the use of the W-M function towards the disorder distribution generation.

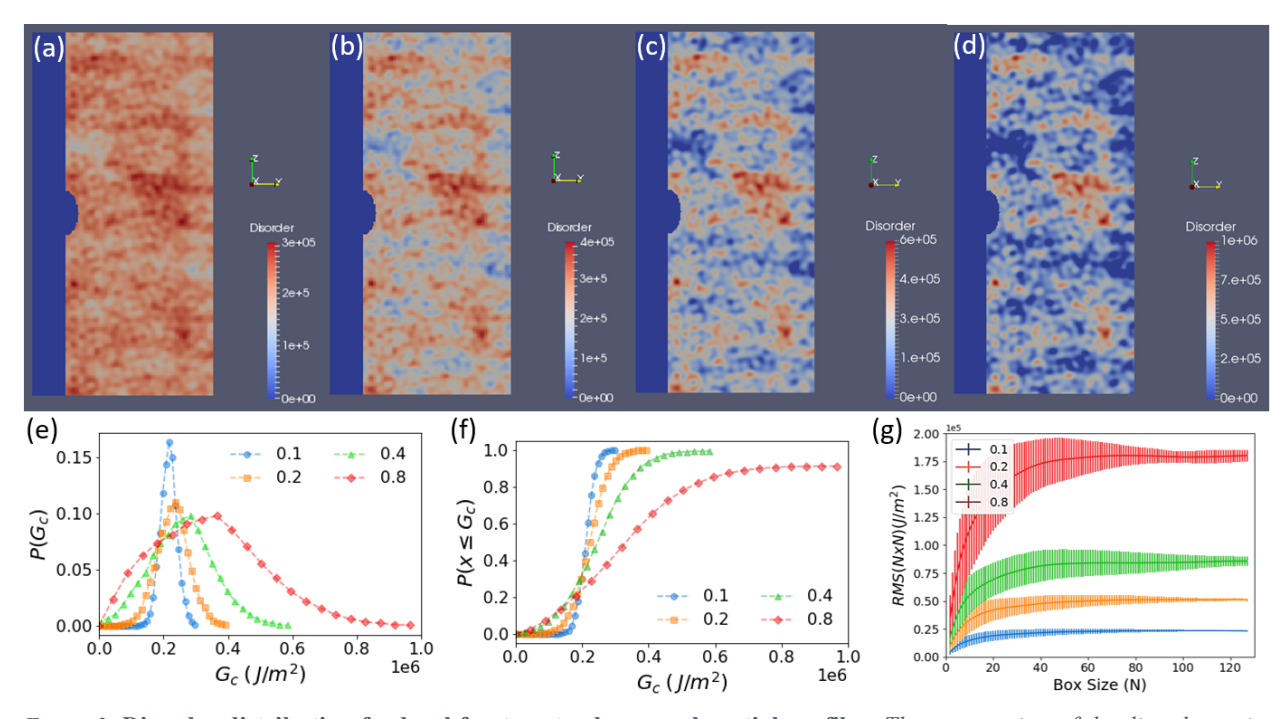


Figure 3: Disorder distribution for local fracture tendency and spatial profiles: The progression of the disorder ratio, R_G , for W=0.125 mm with a system size of $L_x=8$ μ m, $L_y=0.5$ mm, and $L_z=1.0$ mm where (a) has a disorder ratio of 0.1, (b) has a disorder ratio of 0.2, (c) has a disorder ratio of 0.4, (d) has a disorder ratio of 0.8, (e) and (f) are the probability density function (pdf) and cumulative distribution function (cdf), respectively, of the fluctuating phase field energy parameter of each node vs. the phase field energy parameter, and (g) is the autocorrelation lengthscale of the W-M function.

Figure 3 depicts a progression of the increasing R_G . As $R_G \rightarrow 0$, the fluctuations in the critical J-integral value, J_{Ic} , will be relatively small leading to elastic response. As $R_G \rightarrow 1$, the variation in the critical strain energy or material fracture toughness

will overcome the elastic stresses originating from the notch curvature in inducing damage.

Physically, the R_G value allows one to control the variation in the toughness of the material. We choose the mean critical strain energy parameter, G_c , of the material to be a value of 200 kJ/m², rendering the sample quite brittle, more brittle than steel alloys. As Figure 3 shows, our simulations are performed in such a way that the average G_C remains relatively constant as we modify the variance of G_C . In Figure 3, the distribution for $R_G = 0.8$ and W = 0.125 mm exhibits a much larger variation in the range with parts of the distribution having higher values of critical strain energy release rate, indicated by red, versus lower values of critical strain energy release rate, indicated by shades of blue. As R_G increases, the legend's scale maximum is expected to increase as higher values in critical strain energy or fracture energy will be present in the distribution. Furthermore, panel (e) refers to the histogram of the critical strain energy release rate values.

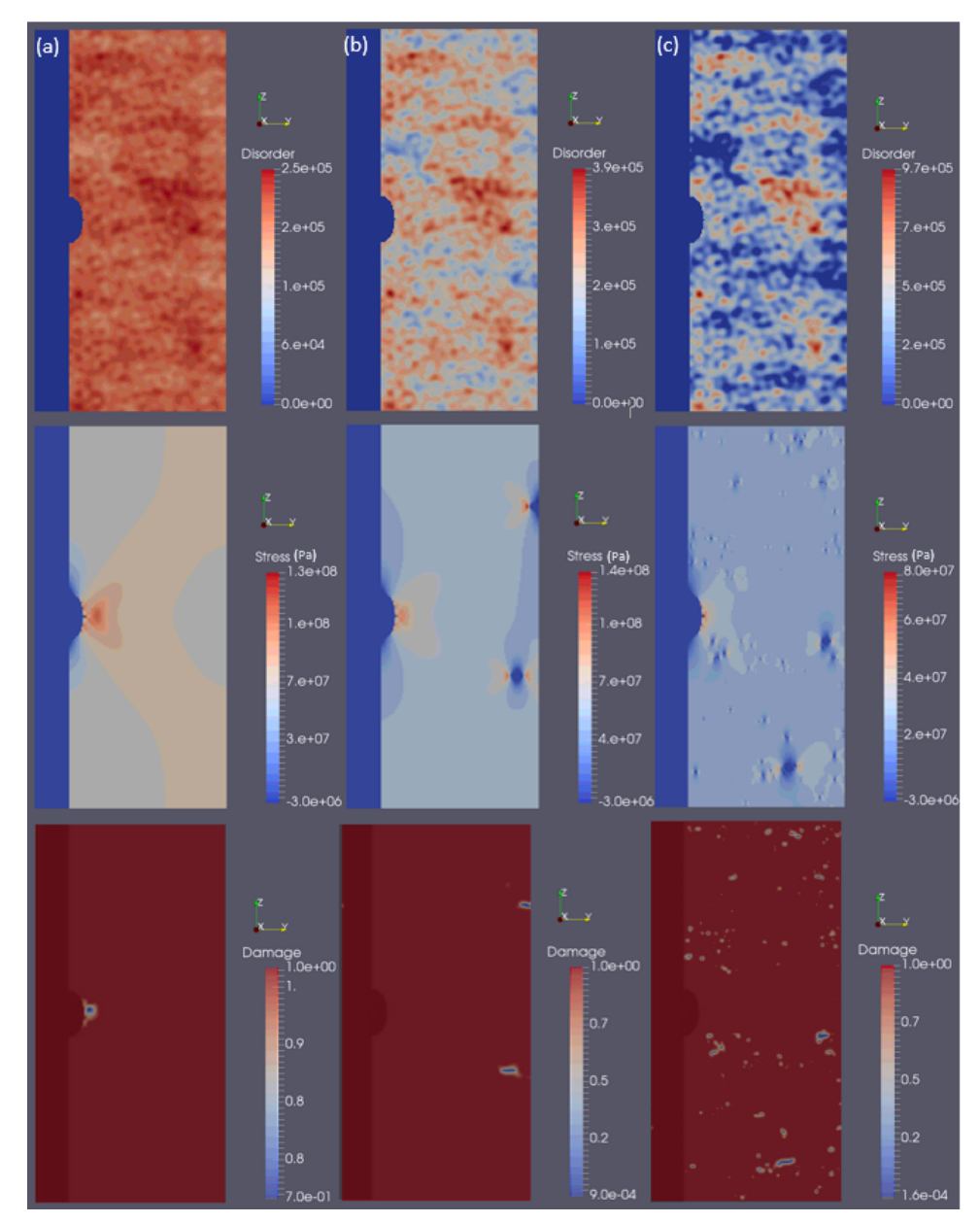


Figure 4: Effect of increasing disorder strength on crack nucleation: Simulations of system size of L_x =8 μ m, L_y =0.5 mm, and L_z =1.0 mm where D=2.995, W = 0.125 mm, and (a) has a R_G of 0.05 (b) has a R_G of 0.2 (c) has a R_G of 0.8 where the disorder, stress and damage distributions are displayed (top, middle, bottom respectively), respectively.

In the presence of disorder, the crack initiation occurs typically at the initial crack tip. In Figure 4, crack initiation as function of disorder is shown: when the R_G value is 0.05 (panel a), while the crack initiated at another location away from the notch tip for R_G of 0.2 and 0.8 from (panels b and c), respectively. It can be seen that the crack propagation was affected by the increased variance in the critical strain energy release rate. At the lower disorder ratio distributions, the crack is rather straight and remains so as it propagates through the specimen. However, as the disorder ratio increases, the observed trend shows that crack nucleation occurs away from the initial notch. Then, at even higher disorder strengths, multiple cracks begin to nucleate across the entire specimen. For the cases where $R_G < 0.2$, we observe that the crack propagates at the notch,

but as it continues through the specimen, the crack's path is altered, moving through areas of lower critical strain energy release rate as a result of the introduced disorder. There is a transition in the behavior: At low disorder ratio R_G, the specimens' exhibit behavior that follows brittle fracture mechanics, nucleating at the notch tip, but, at higher disorder strengths, notch-driven fracture transitions from brittle to a quasi-brittle, disorder-driven fracture with nucleation behavior that is influenced by crystal plasticity.

As we focus closer on this phenomenon with respect to disorder, we examine the damage and stress distributions. However, it is pertinent to this discussion to look at the time of the damage accumulation that causes crack initiation by

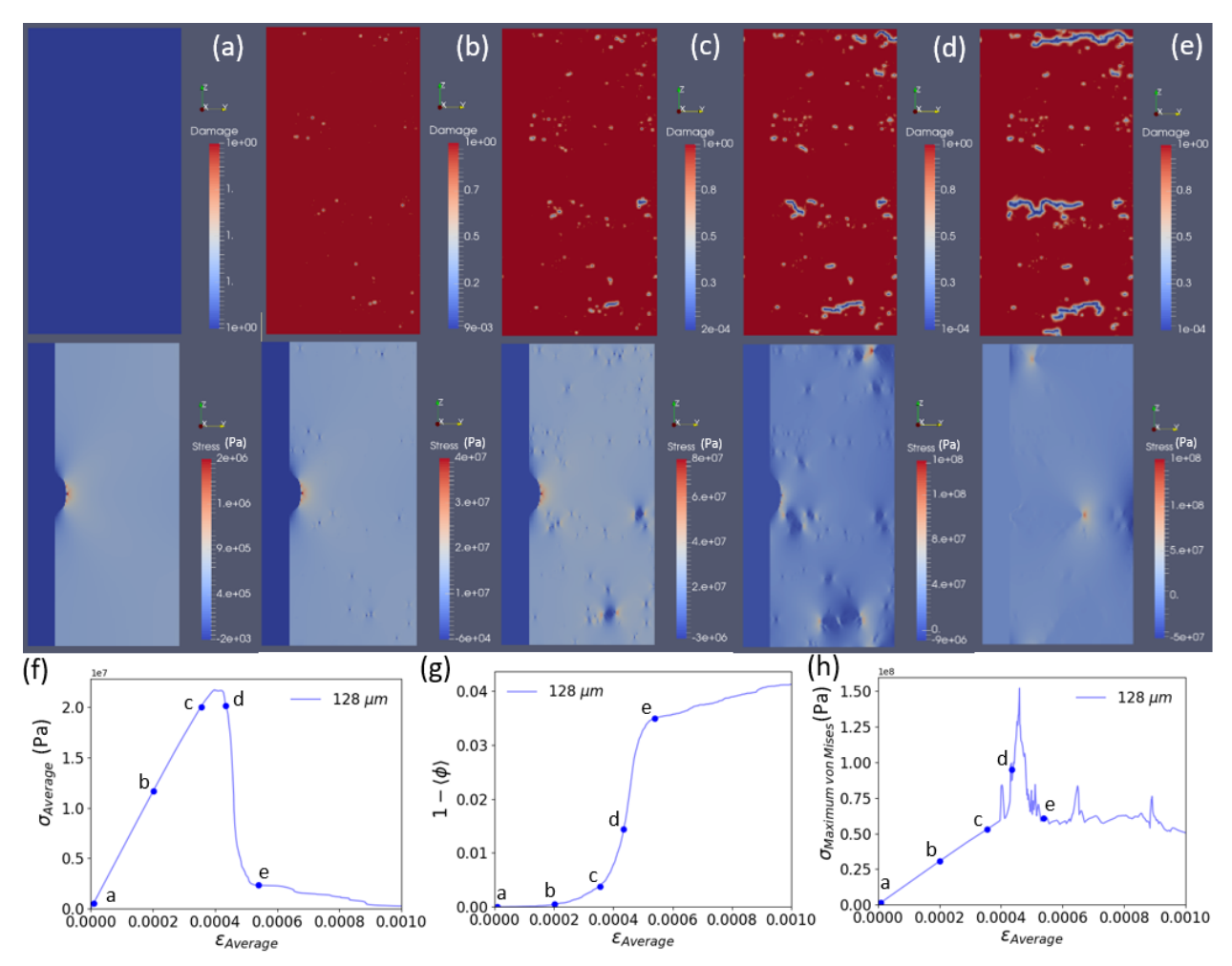


Figure 5: Stress and damage progression in a disordered, notched, crystalline sample: Simulations of system size of L_x =8 μ m, L_y =0.5 μ m, and L_z =1.0 μ m where D=2.995, μ =0.125 μ m, and μ =0.8 where (a) is the undamaged phase, (b) is the early damage phase, (c) is the late damage accumulation phase, (d) is the multiple crack nucleation event, and (e) is the crack propagation where the damage and stress distributions and are displayed (top, middle), respectively, and (f), (g), and (h) are the average stress (Pa) vs. strain, average damage vs. strain, maximum von Mises stress (Pa) vs. strain (bottom) respectively, where the five locations are identified on the curves.

considering various snapshots during the loading of the specimen for the case of W = 0.125 mm and $R_G = 0.8$.

Figure 5 exhibits the fracture behavior as the load case progresses. The undamaged phase, (a), is used as a comparison with the progression of damage and stress distributions. During the undamaged phase, the specimen shows no damage. However, there is a stress concentration at the tip of the notch, as expected, indicating that this location has the highest stress values. As the progression continues, the next phase, (b), reveals that damage has occurred in the bulk of the sample and the stress

has increased at the notch tip. Stress is beginning to increase at multiple locations throughout the sample where the critical strain energy release rate is lower compared to the mean. As loading further continues, damage accumulates and crack initiation occurs, but the crack initiation occurs at multiple locations on the sample, as can be seen in panels (c), (d), and (e). There are several factors that determine the location of the inclusion that propagates through the specimen. It is determined by material properties like critical strain energy release rate, stress distribution at the current load step, statistical modelling, and proximity to other inclusions.

3.2 Width of Notch and its Effects on Crack Initiation and Propagation

The principle theory that guides crack initiation of a notched specimen is fracture mechanics. For our simulations, we analyze the behavior under Mode I fracture where tension or compression is used to initiate a crack. LEFM is used to approximate the stresses at the crack tip. However, it is well recognized that this model is inaccurate in a limited region of the Fracture Process Zone (FPZ) (Bazant 2004). The small scale yielding model for the size of this region can be approximated so that the stresses outside the process zone are accurate. For an ellipsoidal crack shape with initial crack

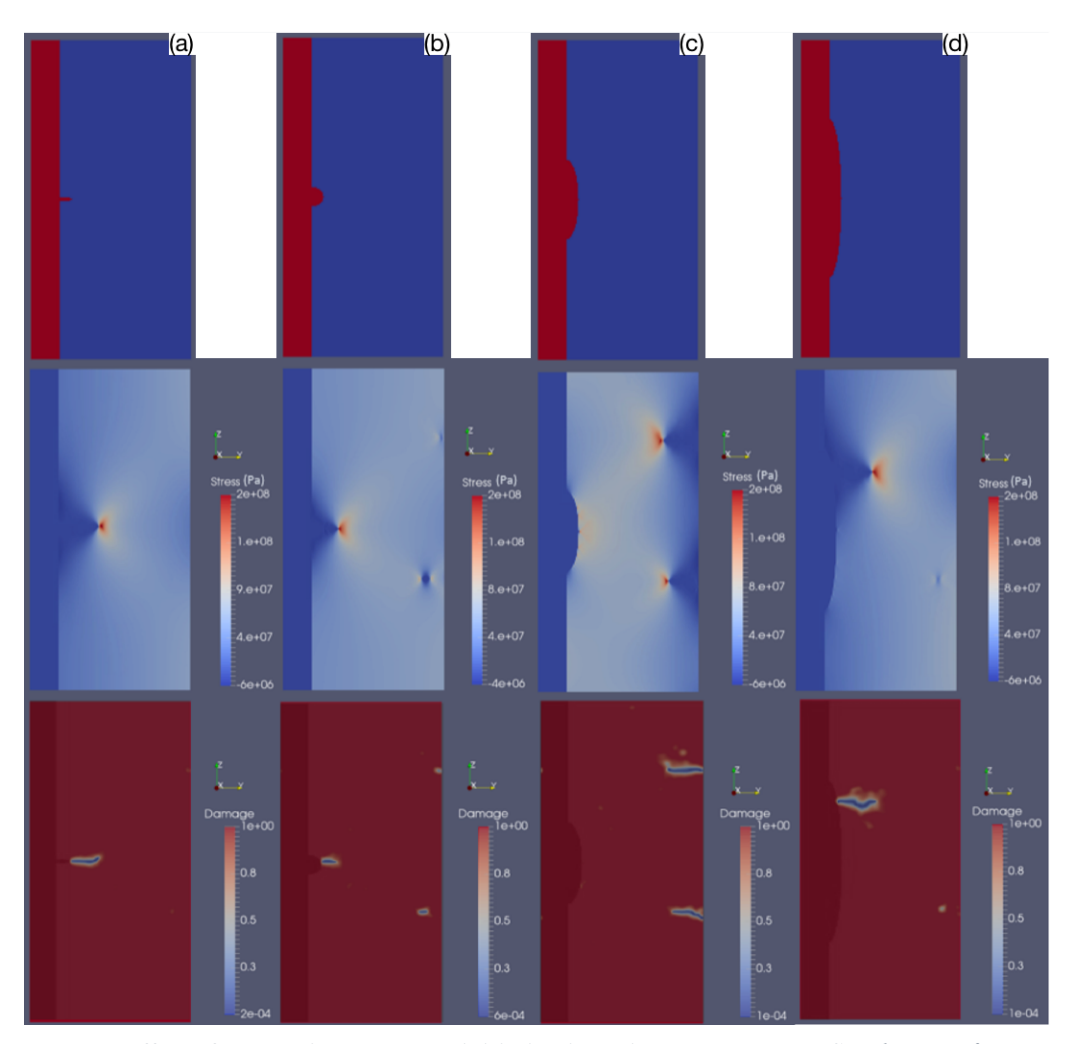


Figure 6: Effect of notch width on crack initiation in a disordered crystal: Simulations of system size of L_x =8 μ m, L_y =0.5 mm, and L_z =1.0 mm where D=2.995, R_G = 0.2, and (a) has a W of 16 μ m (b) has a W of 64 μ m (c) has a W of 0.25 mm (d) has a W of 0.5 mm where the texture, stress and damage distributions are displayed (top, middle, bottom), respectively.

length a, the stress intensity factor at the tip can be approximated by equation 9. But, the stress intensity factor changes everywhere in the specimen as the crack continues to grow.

$$K_I = \sigma_{\infty} \sqrt{\pi a} \tag{12}$$

where σ_{∞} is the tensile stress that the sample is subjected to. As the length of the crack increases, the stress intensity factor at the crack tip will increase. However, crack propagation only occurs in the event that stress intensity factor, K_{IC} (Zehnder 2012). Due to the existence of spatial disorder in the elastic energy release rate, crack initiation occurs within the material bulk due to lower fracture toughness values compared to the notch tip.

At relatively low disorder strengths and low notch widths of 64 μ m or less, crack initiation occurs at the notch, but as the notch width W increases, the location of crack nucleation will deviate from this behavior, occurring within the sample. Figure 6 shows the crack propagation behavior of disorder strength, $R_G = 0.2$, with respect to the various crack widths of 16 μ m, 64 μ m, 0.25 mm, and 0.5 mm. The load case and disorder distributions for these samples were held constant across the simulations. However, there is varying behavior in the crack nucleation location and, as a result, the crack propagation behavior. As explained above, the low crack widths, like (a) and (b), exhibit large stress concentration values at the tip of the notch as the radius of curvature at the crack tip becomes smaller. Upon examination of (c) and (d), the radius of curvature is much larger, allowing for lower stresses at the notch tip compared to the rest of the stresses present in the sample. Instead of crack initiation at the notch tip, nucleation occurs at a location where the critical strain energy release rate in the phase field energy distribution is statistically lower than the critical strain energy release rate at the notch tip. This behavior is observed across the same disorder strength with increasing notch width, and shows that there is a transition from brittle, notch-driven fracture to quasi-brittle, disorder-induced fracture. As a result, the initial notch width in the specimen can be concluded to have a characteristic effect on the crack initiation and propagation behavior.

LEFM yields a predictive behavior of the crack initiation and propagation that can be solved analytically. Figure 6 shows similar characteristics because, when lower disorder strengths are considered, the critical strain energy release rate's fluctuation contribution to the propagation behavior is relatively low once crack initiation occurs at the tip of the notch.

3.3 Average Stress and Damage through the transition from Brittle to Quasi-Brittle Behavior

The transition in the fracture behavior is observed in terms of the average and maximum stresses, average damage, and crack initiation location. It is important to note that the stress at the notch tip, in the absence of disorder, is (Inglis, 1913):

$$\sigma_{max} = \sigma_{\infty} \left(1 + 2\sqrt{a/\rho} \right) \tag{13}$$

Where the stress at the tip of the notch, σ_{max} , is a function of the applied stress, σ_{∞} , the radius of curvature, ρ , and initial crack length, a. The applied stress is the tensile stress response of the sample as it is incrementally loaded at the specified strain rate. The radius of curvature, $\rho = b^2/a$, is a function of the initial crack length and the width of the notch, W = 2b, given that the minor axis of an ellipse is 2b. Inglis' solution expands on the previous work done by Kirsch where he analyzed the solution for a circular notch in the center of a specimen and found the stress around it to be proportionally $\sigma_{max} \sim 3\sigma_{\infty}$ (Kirsch 1898). Thus, the stress at the tip of the ellipse is proportional to the radius of curvature at the tip. Our simulations incrementally increase the strain at a controlled rate. The stress within the material is growing until it reaches the maximum allowable stress, locally. Because of the introduction of a disorder distribution, the maximum allowable stress at any point of the sample is not uniform and the damage or crack may nucleate anywhere in the sample with a low enough critical strain energy release rate G_c . As the damage increases and the crack nucleates, the average stress, maximum stress, and average

damage of every element in the mesh are recorded and the information is processed as the propagation occurs. The sample averages are plotted versus the average strain.

At the point of crack nucleation, there is an event in which the stress decreases sharply. This is, typically, described as a "pop-in" event where a brittle crack begins to nucleate. In figure 7, at lower disorder strengths, the slope of each maximum stress curve is initially increasing steadily for each individual notch width. As disorder and notch width increase, this characteristic, indicative of brittle fracture, begins to soften and disappear. Instead, it is replaced by a sharp increase in maximum stress profile as the crack nucleates. Furthermore, after the crack nucleates, there are stochastic events which

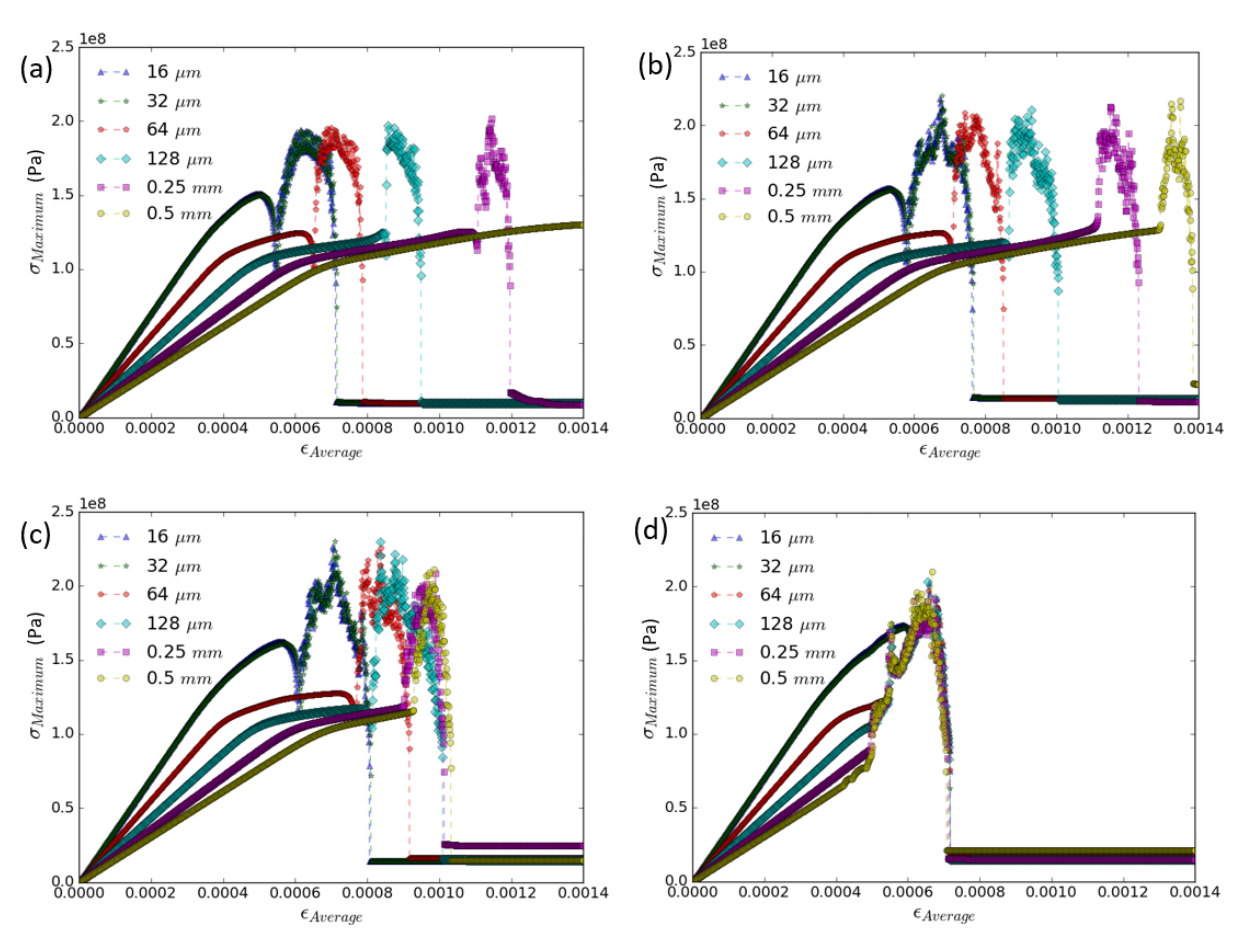


Figure 7: Effect of disorder on maximum stress: The maximum stress of samples of L_x =8 μ m, L_y =0.5 mm, and L_z =1.0 mm where D=2.995 as a function of the average strain with respect to R_G where (a) has a R_G = 0.0, (b) has a R_G = 0.1, (c) has a R_G = 0.2, and (d) has a R_G = 0.4. The figure legends signify the notch width W that varies from 0.25 to 128 μ m.

create avalanches. This is a characteristic of plastic fracture. As deformation continues, the maximum stress continues to obtain high values at the crack tip. Once the crack tip develops, the radius of curvature at the tip becomes very sharp, leading to very high stresses. While it is obvious that the maximum stress is at the crack tip. Due to the discretization unit, a minimum radius of curvature is allowed for the crack tip in the simulation. As the crack propagates, the discretized unit ahead of the crack tip experiences the greatest increase in stress and quickly satisfies criterion for damage in the phase field. Once the crack is initiated and begins to propagate, the specimens for a single disorder strength obtain similar peak values for the fractured tip. As seen in the stress progression of figure 5, once the crack nucleates, the stress profile concentrates at the tip of the crack. After complete failure, the maximum stress decreases sharply to a residual value. At higher disorder strengths,

the maximum stress curves fail to exhibit any of the same trends that the lower disorder strength curves do. The maximum stress values across all notch widths at $R_G = 0.2$ and $R_G = 0.4$ show larger variation in the peak maximum stress values not consistent with the lower disorder strengths. Furthermore, the initial maximum stress decrease at crack initiation dampens out as notch width and disorder strength increase.

At lower disorder strengths, the average stress follows the typical brittle fracture regime with no avalanches or fluctuation in the decreasing average stress. Also, the average stress required for fracture, increases as the notch width increases: Due to the decreasing radius of curvature at the notch tip, the sample requires a larger applied tensile load for damage to occur. At higher disorder strengths, the average stress enters this quasi-brittle fracture regime where there are avalanches as the sample reaches its peak average stress and crack nucleation occurs. Furthermore, this regime, also, produces fluctuations as crack propagation occurs. We focus on the behavior near the brittle-quasibrittle transition.

Overall, the crack initiates at the notch tip when the local critical strain energy release rate is reached and average stress begins to decrease. The average stress curve's response to this event is that the stress decreases relatively quickly, giving brittle signatures. In Figure 8, the behavior of the samples can be characterized as brittle when observing the average stress curves at the lower disorder strengths from (a) and (b). At lower disorder strengths, the sample obtains a small, residual

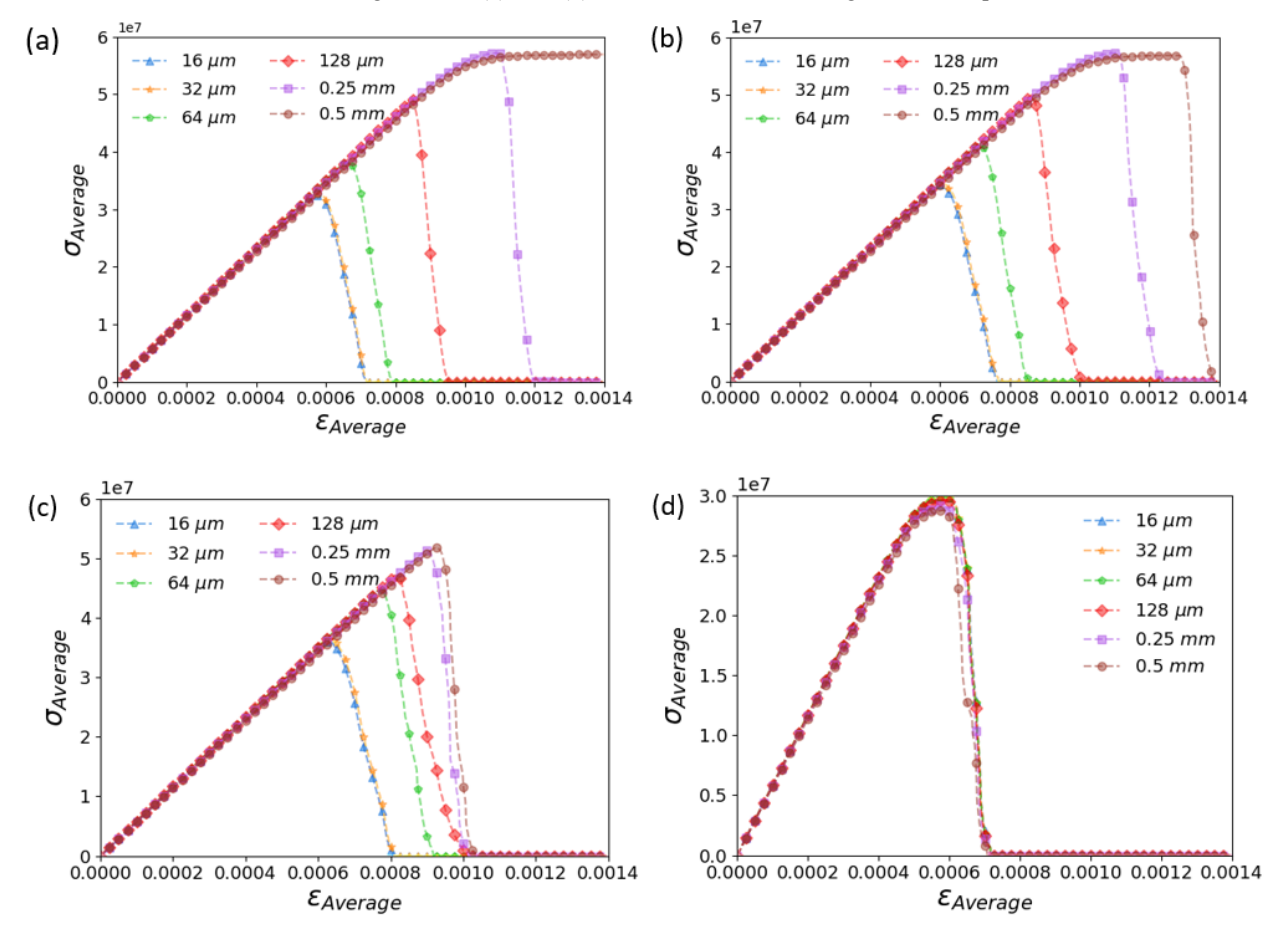


Figure 8:: Effect of disorder on average stress: The average stress of the specimens of L_x =8 μ m, L_y =0.5 mm, and L_z =1.0 mm where D=2.995 as a function of the average strain with respect to R_G where (a) has a R_G = 0.0, (b) has a R_G = 0.1, (c) has a R_G = 0.2, and (d) has a R_G = 0.4. The figure legends signify the notch width W that varies from 0.25 to 128 μ m.

average stress value after complete failure and follows the expected trend: As notch width increases, the maximum average stress increases before crack initiation occurs at the notch tip. With the increasing radius of curvature, the sample exhibits a

plastic characteristic: As the strain is increased, there is no increase with respect to the average stress. However, as the disorder strength increases, the maximum average stress values decrease for higher crack widths and crack initiation occurs earlier in the load case. The fluctuation at which this response occurs is of importance to classifying the fracture behavior. Furthermore, the curves appear to collapse on each other, displaying similar quasi-brittle fracture behavior.

We identify the brittle to quasi-brittle transition as the disorder strength at which there is a clearly observed insensitivity of the maximum average stress before fracture at the notch width. With the quasi-brittle fracture behavior seen at higher disorder, the samples appear to transition from notch-driven to disorder-driven crack initiation around a disorder strength of 0.2. The event size of the fracture was measured and shows a characteristic effect that indicates brittle or quasi-brittle fracture. The measured event size for a brittle sample exhibits a single large stress drop where failure occurs. Moreover, the events are sensitive to the strain applied. However, samples that experience quasi-brittle fracture often exhibit multiple stress drops which are measurable stress events. Therefore, we consider not only the stress event size, but the number of events with their corresponding stress drops.

As the disorder ratio increases, the average stress curves transition from brittle to quasi-brittle fracture, as expected. Figure 9 shows the characteristic effect of brittle and quasi-brittle samples which can be analyzed by measuring the stress events. This is indicated by observing that brittle samples with low disorder only have a single stress event during fracture where stress events are defined as significant stress drops in the average stress profile. Quasi-brittle samples are seen to have multiple stress events as seen in Figure 9a. Though one stress event dominates fracture, the precursor events still have significant stress drops that must be considered. Furthermore, in Figure 9b, the stress events demonstrate clear insensitivity in the average maximum stress at similar strain values. While trivial that crack nucleation depends on the competition

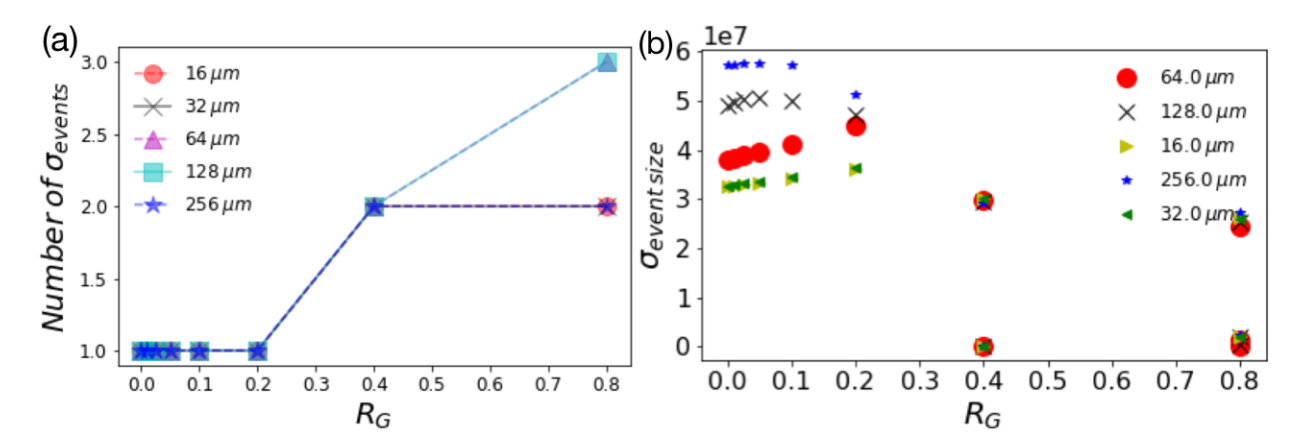


Figure 9: Significant Stress Events for Brittle and Quasi-brittle Fracture: The number and size of the stress events were measured as a function of R_G where (a) is a series of histogram curves for various W and (b) is a plot of the event size for various W. The figure legends signify the notch width W that varies from 16 to 256 μ m.

between local variations in material properties and the notch, it should be noted. As they approach this transition, the disorder introduces stochastic fracture effects in the model material. We do not present the case for which W = 0.5 mm as it is a limit reached in the simulations where the resolution for the discretize notch tip curvature is similar in both cases and, therefore, produces a similar critical disorder strength for the transition to occur.

The peak average stress is used to solve for the critical stress intensity factor as the crack initiates. Therefore, the critical stress intensity factor can be defined as function of the maximum average stress, $\sigma_{\infty,maximum}$, and the crack length, a: $K_{IC} = \sigma_{\infty,maximum}\sqrt{\pi a}$. According to pure elastic arguments, the critical stress intensity factor remains constant as the initial value for a remains constant (Bazant 2004). However, with the contribution of induced-disorder, there is an additional length

scale that must be considered. As disorder strength increases, the theory behind notched-specimen fracture mechanics has less of an impact on the crack initiation and propagation behavior. Instead, the crack nucleation and growth behavior is driven by the fluctuating material toughness energy in the phase field model.

Characterizing the effect of increasing the critical strain energy release rate variance across several system sizes is necessary to understanding how fracture behavior transition is impacted by the sample length, L_y . One way to indicate this is by the difference in the maximum strain, average strain or other observables at fracture, between the very sharp (W = 16 µm) and very thin notch (W = 0.5 mm) cases. This difference can be viewed as an order parameter for the aforementioned phase transition. As in figure 8 for various notch widths, the average stress curves begin to collapse on each other as the disorder strength increases. Data was collected for three system sizes, ranging from L_y of 0.25 to 1.0 mm. Also, disorder strengths were tested for the range 0.0 to 0.8.

As we observed the behavior of the average stress curves (Fig. 8), once the maximum average stress is reached the stress begins to decrease relatively linearly. However, the stress does not obtain a value of zero rather a residual stress value. Figure

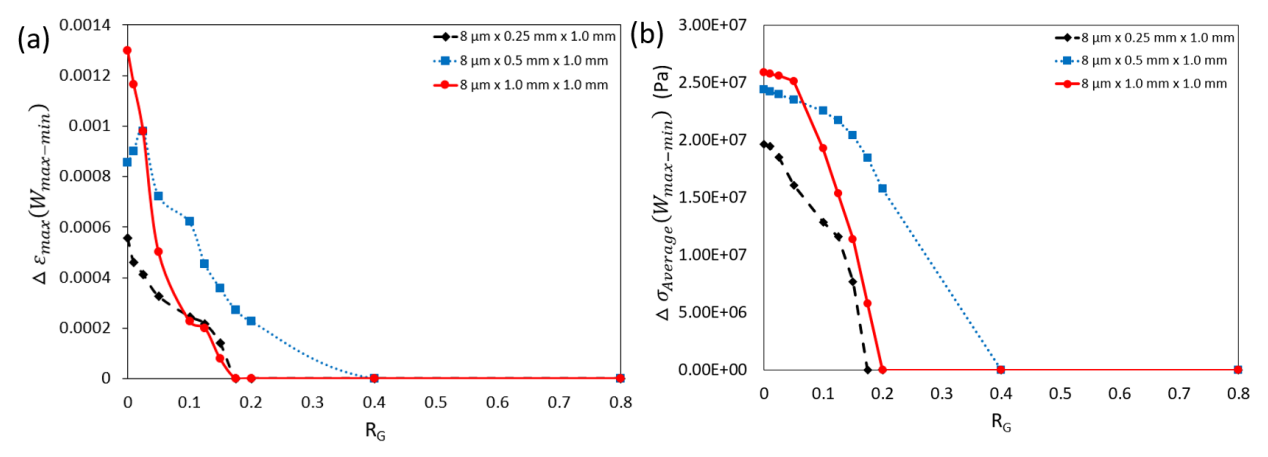


Figure 10: Difference in spatially maximum strain and average stress as a function of disorder strength and maximum and minimum crack width: (a) the difference in the maximum strain of the notch widths of 16 µm and 0.5 mm as a function of disorder (b) the difference in the peak average stress of the notch widths of 16 µm and 0.5 mm as a function of disorder.

10 (a) shows the difference in average strain of the notch width $W = 16 \mu m$ and 0.5 mm at the location of which the residual stress was present. In panel (b) for both cases of $L_y = 0.25$ and 1.0 mm, the average stress curve of notch widths 16 μm and 0.5 mm are very similar in behavior and magnitude, collapsing on each other at approximately same disorder strength. The behavior of these curves exhibit a much shaper decline than $L_y = 0.5 \mu m$ in the maximum difference of average stress for the notch widths. The differences are expected for the fact that disorder is not sample averaged.

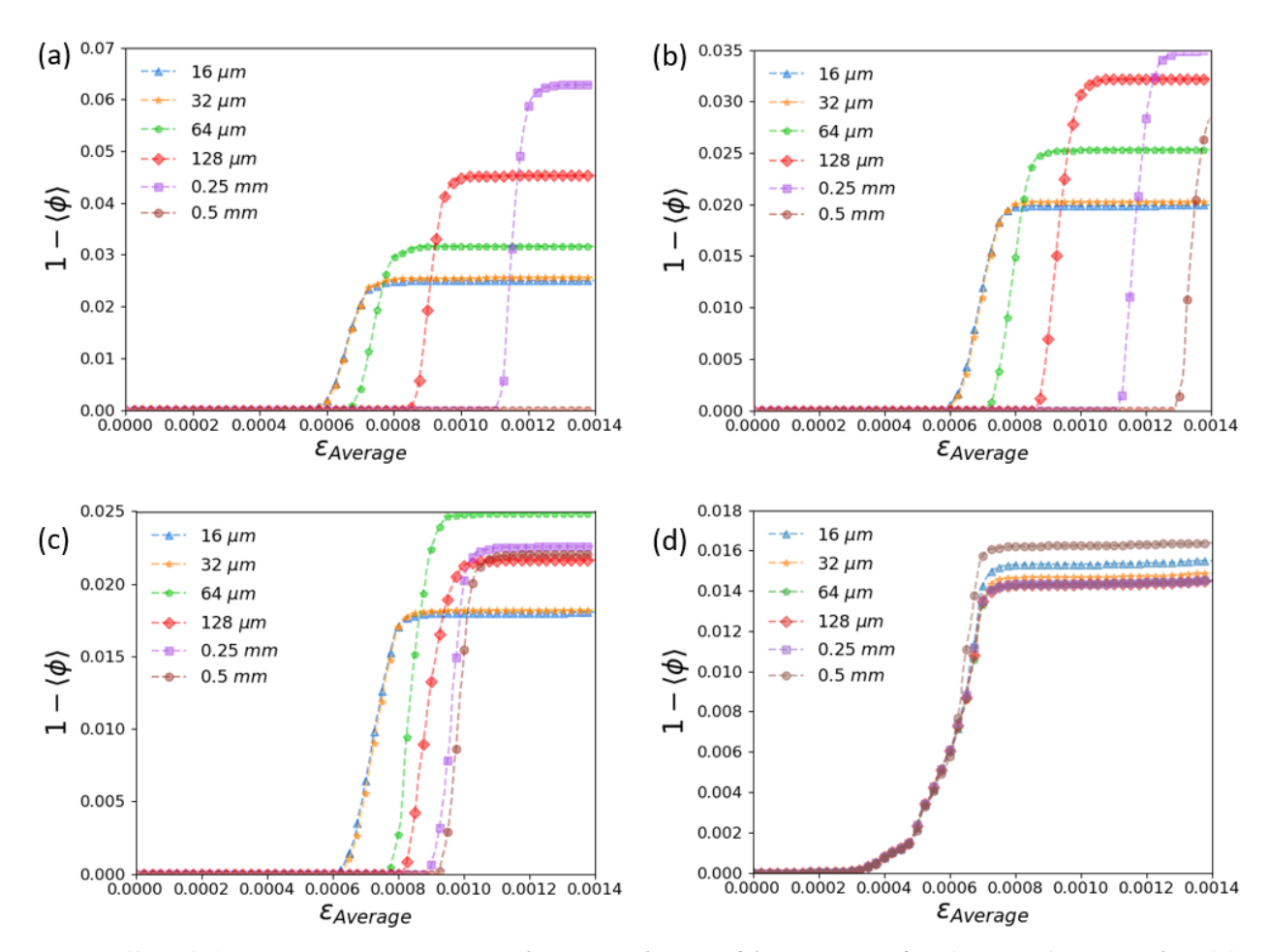


Figure 11: Effect of disorder on average damage: The average damage of the specimens of L_x =8 μ m, L_y =0.5 mm, and L_z =1.0 mm where D=3.995 as a function of the average strain with respect to R_G where (1) has a R_G = 0.0, (2) has a R_G = 0.1, (3) has a R_G = 0.2, and (4) has a R_G = 0.4. The figure legends signify the notch width W that varies from 0.25 to 128 μ m.

In figure 11, the average damage is plotted as a function of the average strain. However, as damage is a local phenomenon, we track how many elements in the Fourier grid exhibit damage as the displacement-controlled loading case affects the phase field energy. The displacement of the total sample is average and the average strain is what we plot with regards to average damage. The disorder strength increases from 0.0 to 0.4. At lower disorder strengths, the behavior is consistent with the observations made in regards to the average stress where it can be characterized as brittle fracture behavior. Also, at relatively low disorder strengths before the transition, the average damage increases as the notch width increases and the crack initiation occurs at a larger strain. The relationship between maximum achieved average damage and the crack width may be described when considering that the strain value at the crack nucleation for higher crack widths is greater than those in the lower crack width's crack nucleation strain values. For lower disorder strengths, where a single crack initiates at the notch tip, the average damage corresponds proportionally to the crack length as no other damage occurs but at the crack tip as it propagates.

As the disorder strength increases, the behavior of the average damage appears to have converged with respect to the time at which crack nucleation occurs. At $R_G = 0.8$, the trend seen at the lower disorders experiences a reversal, so as the crack width increases, the maximum average damage achieved decreases. However, typically, there are visible events at

higher disorder strengths because of the increased stochastic character of the specimen. With regard to the average damage, there are minor fluctuations in the average damage as it exponentially increases to its final failure point. Furthermore, at the higher disorder strengths, the average damage shows a steady increase as the load case continues even after complete failure. This leads to the assumption that there is some residual stress in the sample that is causing some bonds in the material to break at the point of some of the crack fronts that have not fully propagated through the sample. This transfer in trend only further shows the transition from brittle to quasi-brittle fracture from samples at various disorder strengths.

The rate of change of the average stress curves was analyzed by taking the difference of the increments. The difference

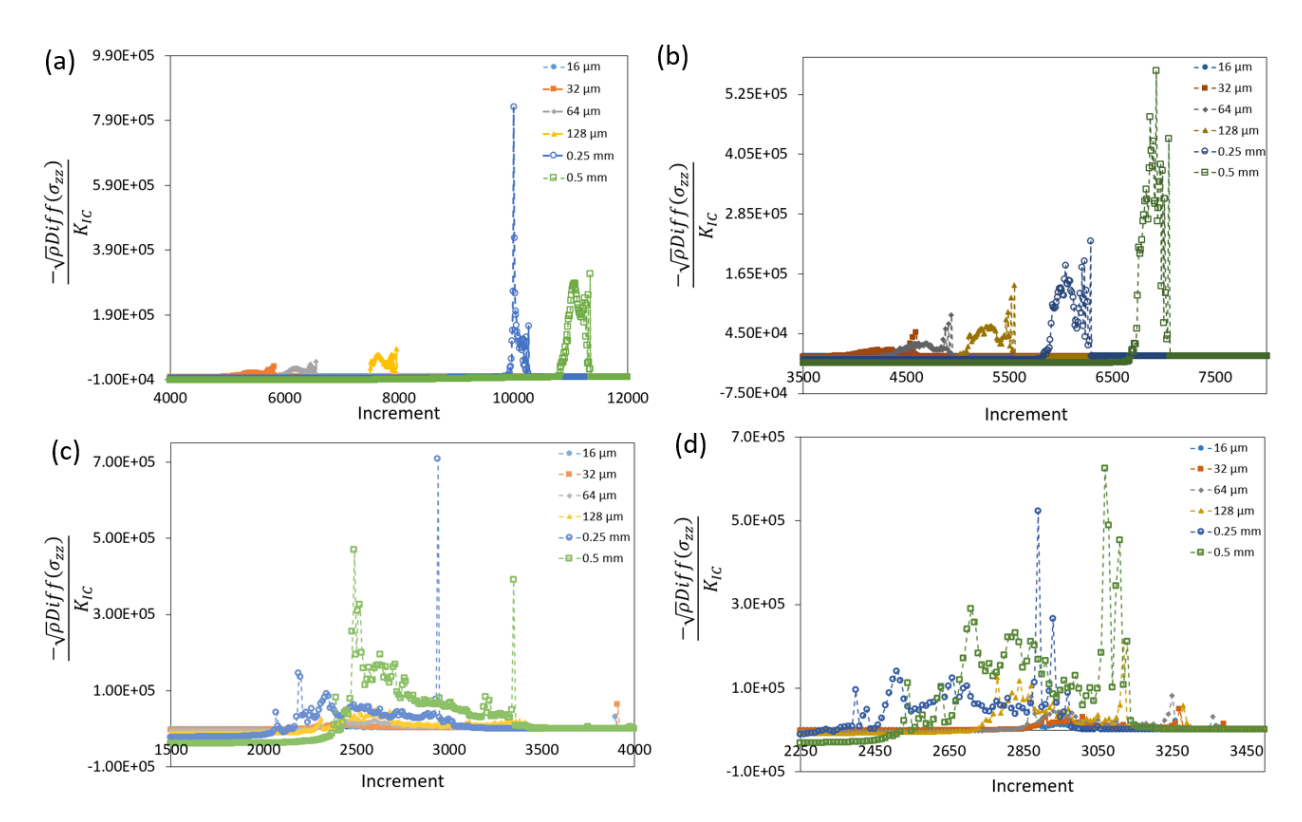


Figure 12: Dimensionless, instantaneous rate of change of the average stress: The dimensionless term for the instantaneous rate of change of average stress of system sizes L_x =8 μ m, L_y =0.25 mm, and L_z =1.0 mm where D=2.995 as a function of the incremental step with respect to R_G where (a) has a R_G = 0.0, (b) has a R_G = 0.1, (c) has a R_G = 0.2, and (d) has a R_G = 0.4. The figure legends signify the notch width W that varies from 0.5 to 128 μ m.

was then multiplied by the square of the radius of curvature and then divided by the critical stress intensity factor in order to produce a non-dimensional parameter.

Figure 12 shows the plots of the non-dimensional parameter for the rate of change of the average stress versus incremental step. Since the simulations are displacement controlled, the behavior of the plots remains unaltered when considering an increment of the average strain across the sample. Fundamentally, the derivative of the average stress plots would show a constant value, initially, as the constant slope of elastic stress remains consistent with the increasing load case. However, after complete failure, the rate of change in the average stress exhibited across all simulations is large. The sharp increase in the rate of change of average stress occurs at about a magnitude of 10² kPa before the parameter becomes dimensionless. This observation indicates that the crack has fully propagated through the sample and the average stress has dropped to values at which it is considered the residual stress. As the disorder strength increases, the event of complete

failure across all crack widths begins earlier in the load case. In panel (a), the rate of change in average stress appears to exhibit the same general trend as the average stress curve. As the disorder strength is increased, the change in the average stress begins to exhibit the same stochastic behavior of the respective disorder strengths.

These abrupt crack-initiation events correspond to avalanche precursors to crack initiation in the model we investigated. The precursors become larger and more intricate as R_G increases, and may amount to 1-5MPa for the model material (*c.f.* Figure 13), a clearly observable range in typical experimental set-ups. However, in the dimensionless parameters, these avalanche precursors' magnitude appear to remain invariant with R_G , suggesting that they may become useful for the prediction of generic crack initiation in intermetallics and other alloys (Ritchie et al. 2001).

4 Conclusions

A simulation-based model of the model material is developed to obtain a better understanding of the realistic response that a specimen would undergo in mode I fracture failure. Analytically, most materials are assumed to be homogenous with constant material properties throughout the sample. However, realistically, through manufacturing and processing, any sample of a material has fluctuations in material properties at the microscale. We considered this assertion valid because if we engineer failure in several alloys under the same loading conditions, then the fracture characteristics will be slightly different from sample to sample. Also, conducting multiple trials in an experiment implies that the behavior of geometrically identical samples will fracture differently.

The Weierstrass- Mandelbrot function was implemented in a material simulation software, DAMASK (Roters et al. 2019), towards the investigation of crack initiation in disordered microstructures that may deform elastically and plastically. A phase field model was implemented to control the critical strain energy release rate of each specimen. Our modeling methods are powerful in that they can carefully describe micromechanical material properties, in a constitutive manner, such as viscoplasticity, hardening, twinning, elastic anisotropy, and they may be used to simulate the fracture behavior. The fractal dimension of the stochastic, microstructural properties, *D*, is increased from 2.85 to 2.995 to increase the magnitude of the critical strain energy release rate fluctuations, in comparison to the artificial magnification of stress fluctuations induced by the modeling resolution of the material geometry. For brittle fracture, the theory of fracture mechanics expects that crack initiation would occur at the notch tip. But, this behavior is, also, exhibited at lower disorder strengths where the critical strain energy release rate variance is not large enough to have an effect on the initial crack nucleation location. At higher disorder strengths, the critical strain energy release rate variance is large enough to induce crack nucleation on the bulk sample where the stresses are higher than those present at the notch tip.

The purpose of increasing the disorder strength in the material simulations is to identify the transition of brittle to quasibrittle fracture behavior. When examining the average stress data, the lower disorder strength and small notch width simulations exhibit behavior more closely characterized as brittle fracture where there were no large or abrupt changes in the average stress curves. At lower disorder strength, but larger initial crack widths, the rate of change in the average stress begins to increase. At higher disorder strengths, all initial crack widths specimens break at relatively the same point but the

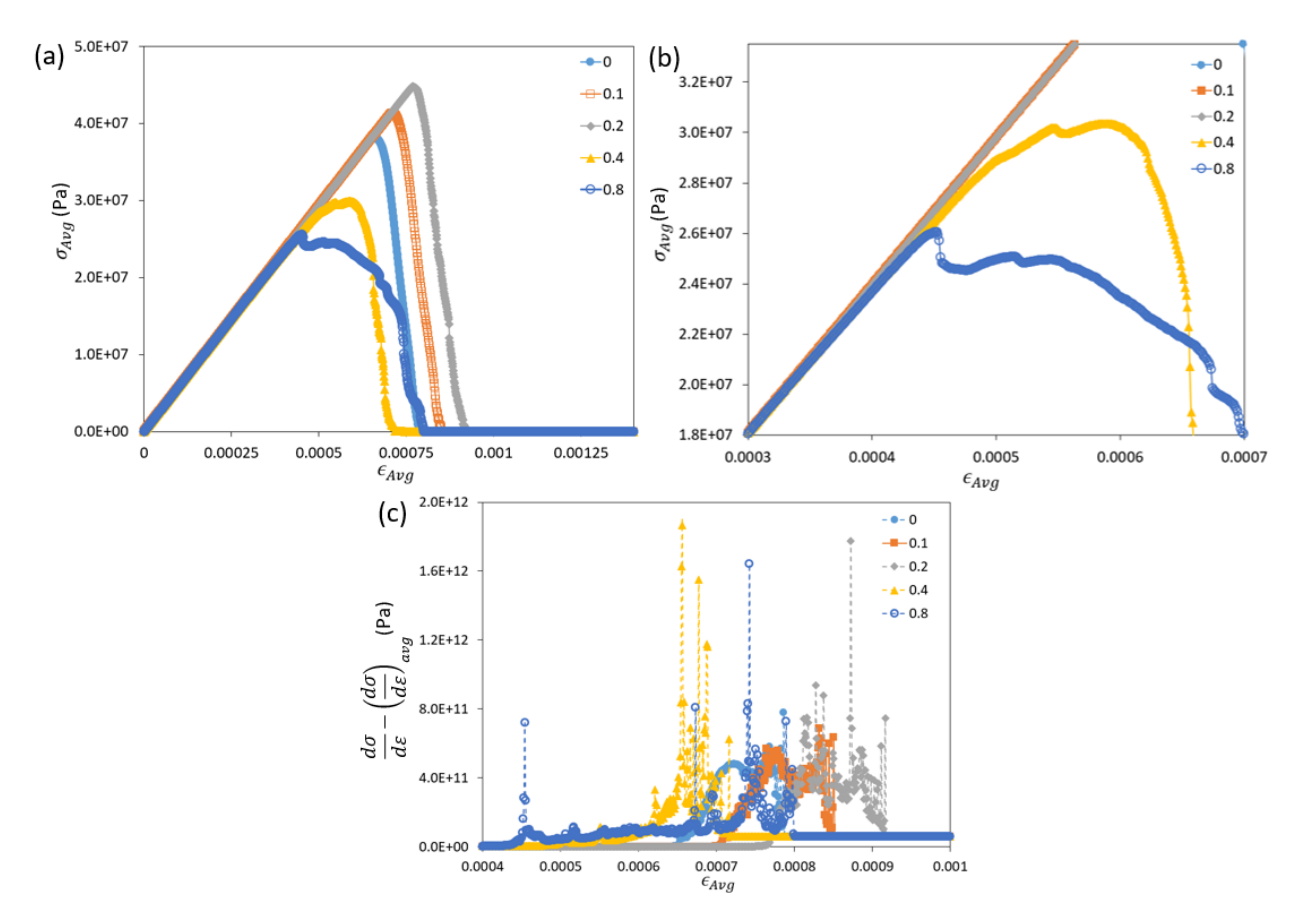


Figure 13: Quantification of the fluctuations at crack nucleation and growth of average stress: Simulations of sample size L_x =8 μ m, L_y =0.5 μ m, and L_z =1.0 μ m where D=2.995 and D=64 μ m as a function of the average strain where (a) is the average stress vs. average strain, (b) is the zoomed-in view of the fluctuations for disorder strengths 0.4 and 0.8, and (c) is the difference in the rate of change of the average stress and the initial rate of change of linear increase in average stress vs. average strain. The figure legends signify the disorder variance ratio R_G that varies from 0.0 to 0.8.

curves collapse on each other. At lower disorder strengths, the peak average damage of the specimen increases as notch width increases, while at higher disorder strengths, the curves across all notch widths begin to collapse on top of each other, exhibiting the same general behavior as the average and maximum stress curves. The maximum value of the maximum stress plots across all of the simulations is approximately 200 *MPa*. All of the specimens exhibit similar maximum stress values because the yield stress and average critical strain energy release rate in the simulations remains constant throughout the simulations. This relation between notch-driven and disorder-driven fracture is identified through the behavior during crack initiation and quantified from parameters like average stress, maximum stress, and average damage. In the future, the aim would be to test several samples of different manufacturing and processing background and characterize the degree of disorder based on the material and fracture behavior. This paper shows that there is a relationship of the fracture behavior between the notch-driven (geometry-based) and disorder-driven (material-based) fracture where it transitions from brittle to

quasi-brittle fracture behaviors for crack nucleation and propagation. These simulations demonstrate that there are observable avalanche precursors that could be tracked in experimental efforts through well controlled experimental setups by just regulating the geometry of the notch on 2D samples. It is plausible that the magnitude of these avalanche precursors extend into a non-trivial scaling function that can be used throughout the critical regime; if that's the case, as this work suggests, then it should become possible to utilize these events towards safe and non-invasive prediction of crack initiation in intermetallics and other disordered brittle materials. Finally, it is important to extend this study into three dimensions and also to ductile fracture, which are straightforward steps, given our current modeling flexibilities.

5 List of Abbreviations

DAMASK: Düsseldorf Advanced MAterial Simulation Kit

2D: Two-dimensional

LEFM: Linear Elastic Fracture Mechanics

FIB: focused ion beam FPZ: Fracture Process Zone

RVE: representative volume element

6 Declarations

6.1 Availability of Data and Materials

The data sets used and/or analyzed during the current study are available from the corresponding author on reasonable request.

6.2 Competing interests

The author(s) declare(s) that they have no competing interests.

6.3 Funding

We would like to acknowledge support from NSF, DMR-MPS, Award No#1709568 "Crack growth during fatigue in Ni superalloys: Physical origin of stochastic jumps and their predictive role using statistical approaches".

6.4 Authors' contributions

CW, SP had the original insight towards this work. PS, FR, SP modified the original DAMASK code towards the purposes of the work. SP produced the simulation data presented in the manuscript. SP, JS analyzed and interpreted the data. All authors read and approved the final manuscript.

6.5 Acknowledgements

We would like to thank M. Alava, C. Reichhardt, H. Song, and E. Van der Giessen for helpful and inspiring comments on this manuscript. We would also like to thank J. El Awady and K. Hemker for inspiring discussions in the beginning of this project. We would like to acknowledge the use of the WVU High Performance Computing facilities for this project. Furthermore,

7 References

Aranson, I. S., Kalatsky, V. A., and Vinokur, V. M. "Continuum field description of crack propagation." *Physical review letters* 85, no. 1 (2000): 118.

Asaro, R. J. "Crystal plasticity." Journal of applied mechanics 50, no. 4b (1983): 921-934.

Asaro, R. J., and Lubarda V.. Mechanics of solids and materials. Cambridge University Press, 2006.

- Bažant, Z. P., and Oh B. H. "Crack band theory for fracture of concrete." *Matériaux et construction* 16, no. 3 (1983): 155-177.
- Bažant, Z. P. "Size effect in blunt fracture: concrete, rock, metal." *Journal of Engineering Mechanics* 110, no. 4 (1984): 518-535.
- Bazant, Z. P. "Fracture in concrete and reinforced concrete." (1985).
- Bazant, Z. P., and P. A. Pfeiffer. "Test of shear fracture and strain-softening in concrete." In *Proceedings of the second* symposium on interaction of non-nuclear munition with structures, Florida, USA, pp. 254-264. 1985.
- Bažant, Z. P., Mazen R. Tabbara, Mohammad T. Kazemi, and Gilles Pijaudier-Cabot. "Random particle model for fracture of aggregate or fiber composites." *Journal of engineering mechanics* 116, no. 8 (1990): 1686-1705.
- Bažant, Z. P. "Size effect aspects of measurement of fracture characteristics of quasibrittle material." *Advanced Cement Based Materials* 4, no. 3-4 (1996): 128-137.
- Bažant Z. P, and Li Z.. "Zero-Brittleness Size-Effect Method for One-Size Fracture Test of Concrete." *Journal of Engineering Mechanics* 122 (5): 458–68. doi:10.1061/(ASCE)0733-9399(1996)122:5(458).
- Bazant, Z. P., and Planas J.. "Fracture and size effect in concrete and other quasibrittle structures." (1998).
- Bažant, Z. P., and Yu Q. "Size effect in fracture of concrete specimens and structures: new problems and progress." *Acta Polytechnica* 44, no. 5-6 (2004).
- Bažant, Z. P., Le J-L., and Bazant, M. Z. "Scaling of strength and lifetime probability distributions of quasibrittle structures based on atomistic fracture mechanics." *Proceedings of the National Academy of Sciences* 106, no. 28 (2009): 11484-11489.
- Brotzu, A., Felli F., and Pilone, D. "Effects of the manufacturing process on fracture behaviour of cast TiAl intermetallic alloys." *Frattura ed Integrità Strutturale: Annals 2014: Fracture and Structural Integrity: Annals 2014* 8 (2014).
- Campbell, J. P., Ritchie, R. O. and Rao, KT V. "The effect of microstructure on fracture toughness and fatigue crack growth behavior in γ-titanium aluminide based intermetallics." *Metallurgical and Materials Transactions A* 30, no. 3 (1999): 563-577.
- Carney, L. R., and Mecholsky, J. J. "Relationship between fracture toughness and fracture surface fractal dimension in AISI 4340 steel." *Materials Sciences and Applications* 4, no. 04 (2013): 258.
- Clemens, H. and Mayer S. "Design, processing, microstructure, properties, and applications of advanced intermetallic TiAl alloys." *Advanced Engineering Materials* 15, no. 4 (2013): 191-215.
- Dimiduk, D. M. "Gamma titanium aluminide alloys—an assessment within the competition of aerospace structural materials." *Materials Science and Engineering: A* 263, no. 2 (1999): 281-288. (Cited by 578)
- Haitham E-K., Horstemeyer M. F., Jordon J. B., and Xue Y. "Fatigue crack growth mechanisms in high-pressure die-cast magnesium alloys." *Metallurgical and Materials Transactions* A 39, no. 1 (2008): 190-205.
- Evans, F. G. Mechanical properties of bone. No. 881. Charles C. Thomas Publisher, 1973.
- Grote, D. L., Park S. W., and Zhou M. "Dynamic behavior of concrete at high strain rates and pressures: I. experimental characterization." International Journal of Impact Engineering 25, no. 9 (2001): 869-886.
- Han, J., Xiao S., Tian, J., Chen, Y., Xu, L., Wang, X., Jia, Y., Du, Z., and Cao, S.. "Grain refinement by trace TiB2 addition in conventional cast TiAl-based alloy." *Materials Characterization* 106 (2015): 112-122.
- Herbold, E. B., Jordan, J. B. and Thadhani, N. N. "Effects of processing and powder size on microstructure and reactivity in arrested reactive milled Al+ Ni." *Acta Materialia* 59, no. 17 (2011): 6717-6728.

- Hu, D. "Effect of composition on grain refinement in TiAl-based alloys." Intermetallics 9, no. 12 (2001): 1037-1043.
- Papanikolaou, S., Yinan C., and Ghoniem N. "Avalanches and plastic flow in crystal plasticity: an overview." *Modelling and Simulation in Materials Science and Engineering* 26, no. 1 (2017): 013001.
- Kim, Y-W., and Dimiduk, D. M. "Progress in the understanding of gamma titanium aluminides." *JOM Journal of the Minerals, Metals and Materials Society* 43, no. 8 (1991): 40-47.
- Kim, Y-W. "Ordered intermetallic alloys, part III: gamma titanium aluminides." *JOM Journal of the Minerals, Metals and Materials Society* 46, no. 7 (1994): 30-39.
- Lapin, J. "TiAl-based alloys: Present status and future perspectives." In *Conference proceedings METAL*, vol. 19, no. 21.5, (2009).
- Lay, S., and Yavari, A-R. "Evidence for disordered character of grain boundaries in a Ni3Al-based alloy during reordering." *Acta materialia* 44, no. 1 (1996): 35-41.
- Mandelbrot, B. B. "Fractals: form, chance and dimension." Fractals: form, chance and dimension., by Mandelbrot, BB. San Francisco (CA, USA): WH Freeman & Co., 16+ 365 p. (1979).
- Mandelbrot, B. B., Passoja, D. E. and Paullay, A. J. "Fractal character of fracture surfaces of metals." *Nature* 308, no. 5961 (1984): 721.
- Moulinec, H., and Suquet, P. "A numerical method for computing the overall response of nonlinear composites with complex microstructure." *Computer methods in applied mechanics and engineering* 157, no. 1-2 (1998): 69-94.
- Ochiai, S., S. Kuboshima, K. Morishita, H. Okuda, and Inoue, T. "Fracture toughness of Al 2 O 3 fibers with an artificial notch introduced by a focused-ion-beam." *Journal of the European Ceramic Society* 30, no. 7 (2010): 1659-1667.
- Ritchie, RO and Peters JO. "Small fatigue cracks: mechanics, mechanisms and engineering applications." *Materials Transactions* 42, no. 1 (2001): 58-67.
- Roters, F., Eisenlohr, P., Hantcherli, L., Tjahjanto, D. D., Bieler, T. R., and Raabe, D. "Overview of constitutive laws, kinematics, homogenization and multiscale methods in crystal plasticity finite-element modeling: Theory, experiments, applications." *Acta Materialia* 58, no. 4 (2010): 1152-1211.
- Roters, F., Diehl, M., Shanthraj, P., Eisenlohr, P., Reuber, C., Wong, S.L., Maiti, T., Ebrahimi, A., Hochrainer, T., Fabritius, H.O. and Nikolov, S., 2019. DAMASK–The Düsseldorf Advanced Material Simulation Kit for modeling multi-physics crystal plasticity, thermal, and damage phenomena from the single crystal up to the component scale. *Computational Materials Science*, *158*, pp.420-478.
- Schlangen, E., and Van Mier, JGMi. "Experimental and numerical analysis of micromechanisms of fracture of cement-based composites." *Cement and concrete composites* 14, no. 2 (1992): 105-118.
- Schlangen, H. E. J. G. "Experimental and numerical analysis of fracture processes in concrete." *HERON*, 38 (2), 1993 (1993).
- Schlangen, Ea, and Garboczi, E. J. "Fracture simulations of concrete using lattice models: computational aspects." Engineering fracture mechanics 57, no. 2 (1997): 319-332.
- Shanthraj, P., Rezvanian, O., and Zikry, M. A. "Electrothermomechanical finite-element modeling of metal microcontacts in MEMS." *Journal of Microelectromechanical Systems* 20, no. 2 (2011): 371-382.
- Shanthraj, P., Sharma, L., Svendsen, B., Roters, F. and Raabe, D. "A phase field model for damage in elasto-viscoplastic materials." *Computer Methods in Applied Mechanics and Engineering* 312 (2016): 167-185.

- Skarynski L, and Tejchman J. "Calculations of Fracture Process Zones on Meso-Scale in Notched Concrete Beams Subjected to Three-Point Bending." European Journal of Mechanics, a/Solids 29 (2010): 746–60. doi:10.1016/j.euromechsol.2010.02.008.
- Stoloff, N. S., Liu, C. T. and Deevi, S. C. "Emerging applications of intermetallics." *Intermetallics* 8, no. 9 (2000): 1313-1320
- Tian, Y., McAllister, D., Colijn, H. Mills, M., Farson, D., Nordin, M. and Babu, S.. "Rationalization of microstructure heterogeneity in Inconel 718 builds made by the direct laser additive manufacturing process." *Metallurgical and Materials* Transactions A 45, no. 10 (2014): 4470-4483.
- Tikhovskiy, I., Raabe, D., and Roters, F. "Simulation of earing during deep drawing of an Al–3% Mg alloy (AA 5754) using a texture component crystal plasticity FEM." *Journal of Materials Processing Technology* 183, no. 2 (2007): 169-175.
- Tseng, A. A. "Recent developments in micromilling using focused ion beam technology." *Journal of Micromechanics and Microengineering* 14, no. 4 (2004): R15.
- Vajpai, S. K., and Ameyama, K. "A novel powder metallurgy processing approach to prepare fine-grained Ti-rich TiAl-based alloys from pre-alloyed powders." *Intermetallics* 42 (2013): 146-155.
- Walsh, P. F. "Fracture of plain concrete." Indian Concrete Journal 46, no. 11 (1972).
- Wang, L., Shen, J., Zhang, Y., and Fu, H. "Microstructure, fracture toughness and compressive property of as-cast and directionally solidified NiAl-based eutectic composite." *Materials Science and Engineering: A* 664 (2016): 188-194.
- Weierstrass, K. "Uber continuierliche Functionen eines reellen Argumentes, die für keinen Werth des lezteren einen bestimmten Differentialquotient besitzen." *Math. Werke II* (1895).
- Xie, J., Tian, S., Zhou, X., Li, J., and Wang, X. "Microstructure and enduring fracture features of FGH95 Ni-base superalloy." *Rare Metals* 30 (2011): 447-451.
- Zehnder, A. T. "Fracture Mechanics (Lecture Notes in Applied and Computational Mechanics)." (2012).
- Zhu, L., Xu, Z. F., Liu, P. and Gu, Y. F. "Effect of processing parameters on microstructure of laser solid forming Inconel 718 superalloy." *Optics & Laser Technology* 98 (2018): 409-415.